JOURNAL OF SYNCHROTRON RADIATION
ISSN 1600-5775

Light source based on a 100 mm-long monolithic undulator magnet with a very short 4 mm-period length

Shigeru Yamamoto,[a,b]* Shigeru Kashiwagi,[c] Shinichi Masuda,[a] Nobuhiko Nakanii,[d] Tomonao Hosokai,[e] Masaki Kando,[d] Toshiya Muto,[f] Ken-ichi Nanbu,[f] Fujio Hinode[f] and Hiroyuki Hama[f]

[a]Photon Factory, Institute of Materials Structure Science, High Energy Accelerator Research Organization, KEK, 1-1 Oho, Tsukuba, Ibaraki 305-0801, Japan, [b]Department of Materials Structure Science, The Graduate University for Advanced Studies, SOKENDAI, 1-1 Oho, Tsukuba, Ibaraki 305-0801, Japan, [c]Research Center for Electron Photon Science, Tohoku University, 1-2-1 Mikamine, Taihaku-ku, Sendai, Miyagi 982-0826, Japan, [d]Kansai Photon Science Institute, National Institutes for Quantum and Radiological Science and Technology, 8-7-1 Umemidai, Kizugawa, Kyoto 619-0215, Japan, [e]Graduate School of Engineering, Osaka University, 2-1 Yamamdaoka, Suita, Osaka 565-0781, Japan, and [f]Research Center for Electron Photon Science, Tohoku University, 1-2-1 Mikamine, Taihaku-ku, Sendai, Miyagi, Japan.
*Correspondence e-mail: shigeru.yamamoto@kek.jp

Received 18 April 2019
Accepted 21 September 2019

Edited by M. Yabashi, RIKEN SPring-8 Center, Japan

Keywords: synchrotron light source; undulator; very short period length.

A novel method to fabricate undulator magnets of a-few-millimetre-period length is being explored. Plate-type magnets, 100 mm-long with 4 mm-period length, have been successfully fabricated. They produce an undulator field of approximately 3 kG at a gap of 1.6 mm. Prototype undulators based on this technology have been constructed. Field measurements and characterization show that the quality of the undulator field of these plate magnets is sufficient for an undulator light source, and the calculated spectrum shows that the fundamental radiation emitted from this field is quite satisfactory. Test experiments for light generation using a real electron beam have been carried out at a test accelerator at the Research Center for Electron Photon Science (ELPH), Tohoku University, Japan, which is able to realize optics conditions to accept a very short gap of ~1.6 mm. First observation and characterization of blue light was successfully accomplished.

1. Introduction

Through the progress of synchrotron light sources over the years, light source developers have always received demands to reach shorter wavelengths in order to expand research fields (*e.g.* Yamamoto *et al.*, 1992; Hara *et al.*, 1998; Wallén *et al.*, 2006; Yamamoto *et al.*, 2010; Calvi *et al.*, 2013; Ivanyushenkov *et al.*, 2015; Benabderrahmane *et al.*, 2017). Synchrotron radiation with shorter wavelengths can be obtained with shorter period lengths for the undulators at a given energy of the electron beam. The wavelength λ_k of the kth harmonic of the undulator radiation observed at radial angle θ with electron beam energy γ is given by (Hofmann, 1978)

$$\lambda_k = \frac{\lambda_u}{2k\gamma^2}\left(1 + \frac{K^2}{2} + \gamma^2\theta^2\right). \quad (1)$$

Here K is the deflection parameter proportional to the period length λ_u and strength B_0 of the periodic magnetic field of the undulator,

$$K = 93.4 B_0\,[\mathrm{T}]\,\lambda_u\,[\mathrm{m}]. \quad (2)$$

Fig. 1 summarizes the history of efforts to shorten the period lengths of undulators at the Photon Factory (PF), High Energy Accelerator Research Organization, KEK, Japan. Since the

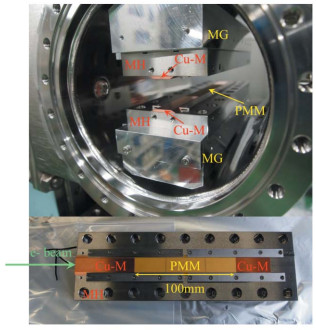

Table 1
Examples of short-period undulators with λ_u of less than 20 mm.

PM, SCM and CPM denote permanent magnet, superconducting magnet and cryogenic permanent magnet, respectively. Here, λ_u is the period length, N is the number of the period, Gap_{min} is the minimum gap, B_{max} and K_{max} are the peak magnetic field and the deflection parameter obtained at the minimum gap.

Facility	Name†	Type	λ_u (mm)	N	Gap_{min} (mm)	B_{max} (T)	K_{max}
KEK-PF	SGU#17 [*1]	PM	16	29	4	0.92	1.374
KEK-PF	SGU#01 [*1]	PM	12	39	4.5	0.70	0.781
LSNS II	IVU18 [*2]	PM	18	>55	5.6	0.95	1.60
SACLA	BL1 [*3]	PM	18	277	3.5	1.3	1.8
MAX IV	SCU14.0 [*4]	SCM	14	214	4.4	1.70	2.21
APS	SCU0 [*5]	SCM	16	20.5	9.5	0.64	0.956
KIT-ANKA	SCU15 [*6]	SCM	15	100.5	8	0.73	1.02
BESSY II	U17 [*7]	CPM	17	88	5.5	1.12	1.78
ESRF	3rd CPMU [*8]	CPM	14.4	138	4.5	1.22	1.51
SLS	U14 [*9]	CPM	14	120	3.8	1.19	1.55
SOLEIL	U18 [*10]	CPM	18	107	5.5	1.152	1.936

† Undulator parameters are reported in the literature: [*1](Yamamoto *et al.*, 2007, 2010); [*2](Tanabe *et al.*, 2017); [*3](Tanaka *et al.*, 2012; Otake, 2012); [*4](Wallén *et al.*, 2006); [*5](Ivanyushenkov *et al.*, 2015); [*6](Casalbuoni *et al.*, 2016); [*7](Hendel *et al.*, 2016); [*8](Chavanne *et al.*, 2015); [*9](Calvi *et al.*, 2013); [*10](Benabderrahmane *et al.*, 2017).

beginning of the PF operation, the period length of the undulators has decreased from around 100 mm to 50 mm in the out-of-vacuum (standard) undulator case, whereas in the in-vacuum case it has decreased from 40 mm to 10 mm.

In-vacuum undulators are advantageous for reducing the period lengths. They were originally invented and developed at PF-KEK (Yamamoto *et al.*, 1992, 1993) in order to obtain shorter wavelengths or higher-energy photons. The undulator magnets were incorporated in the vacuum of the light source accelerator. This method allowed one to utilize the shortest period length of the undulator field which could be produced by the latest magnet materials available at the time. The first important achievement was the production of a successful in-vacuum undulator with a period length of 40 mm which was installed in the 6.5 GeV Photon Factory-Accumulation Ring (PF-AR) (Yamamoto *et al.*, 1992) for the Mössbauer beamline (Yamamoto *et al.*, 1993). This was followed by several more in-vacuum undulators with the same period length of 40 mm installed in the PF-AR, and was followed by several in-vacuum short-gap undulators (SGUs) installed in the 2.5 GeV PF ring. The latter had period lengths of 12–20 mm and were capable of producing hard X-rays with the third or fifth (or higher) harmonics (Yamamoto *et al.*, 2007, 2010). The above developments are summarized in Fig. 1.

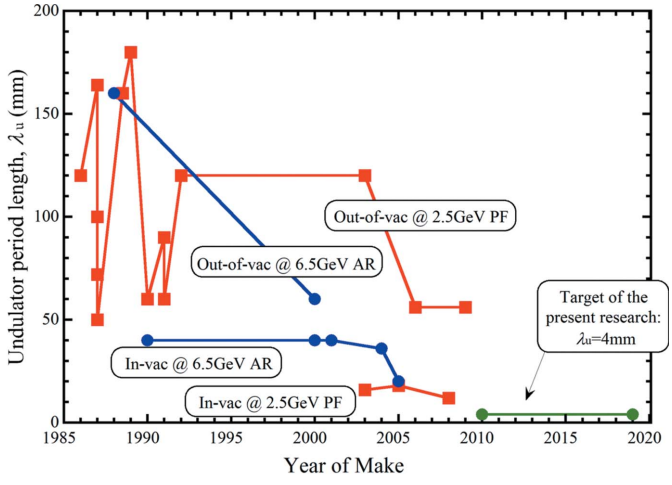

Figure 1
Summary of the development of the reduction of period length of undulators over the years at the Photon Factory (PF), KEK. Red lines indicate the history at the 2.5 GeV PF, and blue lines indicate the history at the 6.5 GeV PF-Accumulation Ring (PF-AR). Out-of-vac and In-vac mean the out-of-vacuum and in-vacuum undulators, respectively. The green line indicates the target of the present research of a-few-millimetre-period undulators.

The technology of in-vacuum undulators spread globally and was transferred to other institutes from the PF. Research and development for the in-vacuum undulators have continued not only at the PF but also at third-generation light sources (Hara *et al.*, 1998; Chavanne *et al.*, 2003). They were also employed at compact third-generation sources (Wallén *et al.*, 2006; Calvi *et al.*, 2013; Tanabe *et al.*, 2017) and an X-ray free-electron laser facility (Tanaka *et al.*, 2012). During the development of these facilities, reduction of the period lengths of the undulators proceeded largely. Period lengths around or below 20 mm are very common in these facilities. To achieve this, the proposal and realization of cryogenic undulator technologies was very important (Hara *et al.*, 2004; Calvi *et al.*, 2013; Benabderrahmane *et al.*, 2017) as one of evolutions of the in-vacuum undulators. The development of superconducting undulators was another important solution for the reduction of the undulator period lengths (Ivanyushenkov *et al.*, 2015; Casalbuoni *et al.*, 2016). Table 1 summarizes and exemplifies specifications of the above-mentioned undulators which have period lengths of less than 20 mm.

As the newest breakthrough along the direction discussed above, we have been developing a novel method to construct undulators with period lengths of a few millimetres (Yamamoto, 2013, 2014, 2015, 2016). The development is underway for a plate monolithic magnet (PMM), 100 mm long in the longitudinal direction with 4 mm as the current target for the period length. The 4 mm-period length was selected since 12 keV radiation can be obtained with the first harmonic of this undulator in the 2.5 GeV accelerator which has the same electron beam energy as the PF, whereas higher harmonics

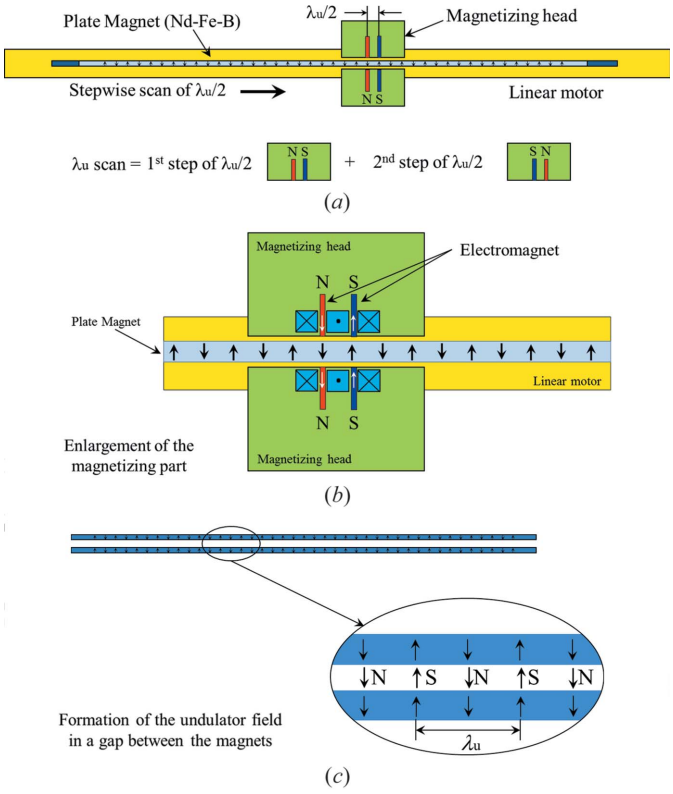

Figure 2
(*a*) Schematic illustration of the perpendicular magnetization of the PMM. (*b*) Enlargement of the magnetizing part. (*c*) Formation of an undulator field with perpendicular magnetization.

would be needed for the PF's current SGUs to achieve this photon energy (Yamamoto *et al.*, 2007, 2010). A multi-pole magnetizing technique was applied to magnetize a PMM; a 4 mm-period magnetic field was generated by pulsed electromagnets and was transcribed into the PMM as shown in Fig. 2. This procedure allows the generation of an undulator field in a very short gap between a pair of opposing PMMs. Thus, these undulators should be operated with a gap much shorter than that of ordinary undulators. They would be very useful when a light source accelerator would be optimized to allow a very short gap; the short gap is required for the operation of the undulators based on the PMM. Further, the present method to obtain a-few-millimetre-period lengths enforces a reduction in the peak magnetic field. It is expected to be at least 30% lower than with the conventional method, due to a fewer number of effective poles per period (= 2), in contrast to that in the conventional Halbach method (= 4) (Halbach, 1981). In this article, the method to obtain a-few-millimetre-period magnetic field is described, and the current achievements are presented with test results.

2. Fabrication of monolithic undulator magnets with a-few-millimetre period

The state-of-the-art undulators are ordinarily fabricated by aligning magnet blocks on a pair of rigid girders. They are shaped very accurately and usually mounted on non-magnetic holders. Shortening of the period length λ_u of the ordinary undulator is accomplished by reducing the size of the magnet blocks while maintaining the accuracy in terms of the ratio of the error in block size and λ_u. However, when λ_u goes down to less than 10 mm, fabrication of accurate magnet blocks becomes rather difficult while keeping the above accuracy. Further, the components for assembling these blocks and their holders, such as screw bolts, become too small to be practical.

Contrary to the standard method mentioned above, we have been developing a completely new method to realize undulator magnets with period lengths of a few millimetres. Here, a multi-pole magnetizing method is applied for magnetizing a thin PMM. After several trials reported elsewhere (Yamamoto, 2013, 2014, 2015), we finally managed to devise the present method (Yamamoto, 2016, 2018), details of which are shown in Fig. 2. The PMM made of Nd–Fe–B type material was embedded between a pair of magnetizing heads of electromagnets. It was longitudinally driven by a linear motor in steps and magnetized with a periodic spacing by the fixed head as shown in Figs. 2(*a*) and 2(*b*). The step width of the moving plate was set to half of the period length of the magnetic field. At each step of the plate movement a current pulse was applied to the head, and was reversed in direction at the next step to form the undulator field. Thus the periodic magnetic field was transcribed onto the PMM.

In the geometry shown in Fig. 2 the magnetization direction is perpendicular to the plate surface (the perpendicular case). This geometry is similar to that of the perpendicular magnetic recording method in a recording media. The other geometrical case (the longitudinal case) is also possible, when the current direction in one of the electromagnets is reversed with respect to that in the other magnet. In this case the magnetization is formed along the plate surface as in longitudinal magnetic recording (Yamamoto, 2013).

Accuracy in the period length of the magnetic field transcribed to the PMM is mainly determined by the accuracies of both the spacing of the pole piece in the head and the step width of the plate movement driven by the linear motor. It is controlled by a closed-loop scheme with an accuracy of 0.003 mm. We also devised a magnetizing head in which accurate pole spacings were achieved. Thus, the accuracy of the field strength achieved is essentially determined by the precision in the period length and the quantity of the electric charge applied to the head at each step.

The PMMs, 100 mm long with 4 mm-period length, are shown in Fig. 3 after magnetization. They are made of NEOMAX-37SH (Hitachi Metals Co. Ltd) and coated with TiN for vacuum sealing. Here, the PMMs are incorporated in a case made of an acrylic resin to isolate each other and to avoid any accidents. The magnetic field pattern is seen through a magnetic viewer sheet for one of the PMMs in Fig. 3. The present successful magnetization reveals that a 'monolithic' undulator magnet is now available if the number of periods of 25 available with the 100 mm-long PMM is enough for practical use at synchrotron radiation facilities. Further, the fabrication of these PMMs can be useful for reducing the undulator size and for conservation of resources, such as rare-

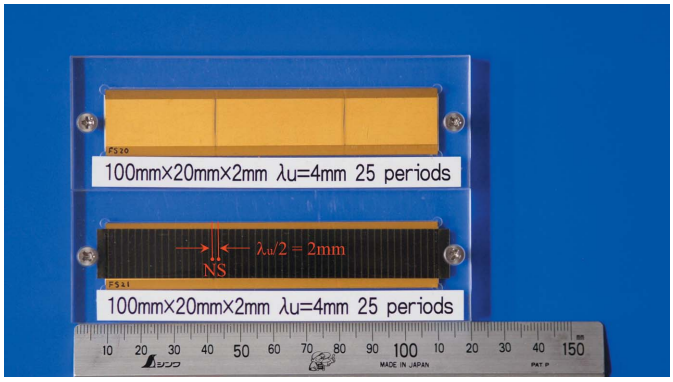

Figure 3
The 100 mm-long PMMs after magnetization with a period length of 4 mm, made of Nd–Fe–B material and coated with TiN. These PMMs are paired and opposed to form the undulator field. The lower PMM is covered by a magnetic viewer sheet, and the magnetic field pattern can be seen through it.

earth elements, needed as the major components of Nd–Fe–B material.

3. Generation and characterization of the undulator field

After magnetization, a pair of these PMMs are combined with faces opposing each other, and thus the undulator magnetic field is generated in the short gap between the PMMs. The quality of the 'monolithic' undulator magnet is examined by measuring the magnetic field. The vertical magnetic field is measured by a Hall sensor, whose active area is 0.05 mm × 0.05 mm.

The results of the measurements on the undulator field having a 4 mm-period length are shown in Fig. 4 for a pair of 100 mm-long PMMs (numbered FS16 and FS19), which were used in the light observation experiment described in Section 5, and different from the pair shown in Fig. 3. Fig. 4(*a*) shows the undulator field at several different gaps, and Fig. 4(*b*) shows the calculated electron orbit in this field at the same gaps for an electron energy of 2.5 GeV. By optimizing the longitudinal relation between the magnetizing head and the PMM, we have a nearly symmetric field distribution in the longitudinal direction with respect to the center of the PMM as shown in Fig. 4(*a*). An anti-symmetric distribution is also possible by optimizing this relation. The amplitude of the magnetic field shown in Fig. 4(*a*) is plotted as a function of the gap in Fig. 4(*c*). A magnetic field of approximately 3 kG was obtained at a gap of 1.6 mm. In Fig. 4(*c*) the measured data are compared with calculated gap–field relations. The calculation is made according to the analysis given by Halbach (1981), on the assumption that NEOMAX-37SH material is used and magnetization is complete. Here we present two results: one corresponds to a case with the same structure as the present PMM where two effective poles per period exist, and the other to a case of the normal Halbach undulator where four effective poles per period exist. The former is shown by a solid curve and the latter by a dashed curve. We note differences

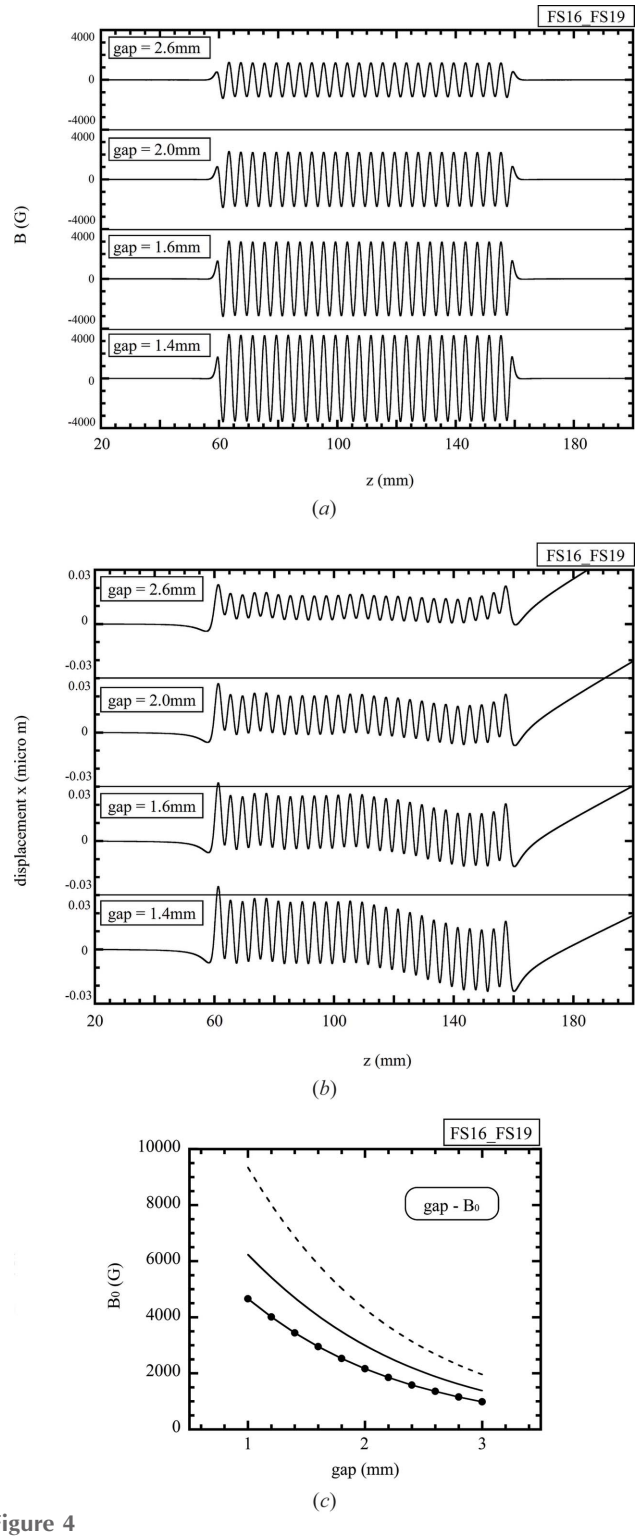

Figure 4
(*a*) Undulator field of the pair of 100 mm-long PMMs (numbered FS16 and FS19) with a period length of 4 mm measured at gaps of 1.4, 1.6, 2.0 and 2.6 mm. (*b*) Calculated orbit of an electron with 2.5 GeV energy in the undulator field at the same gaps. (*c*) Amplitude of the magnetic field as a function of the magnet gap (solid circles). The calculated gap–field relation is also shown. The solid curve represents a case with the same structure as the present PMM where two effective poles per period exist, and the dashed curve represents a case of the normal Halbach undulator where four effective poles per period exist. The calculation was made on the assumption that NEOMAX-37SH material is used and magnetization is complete.

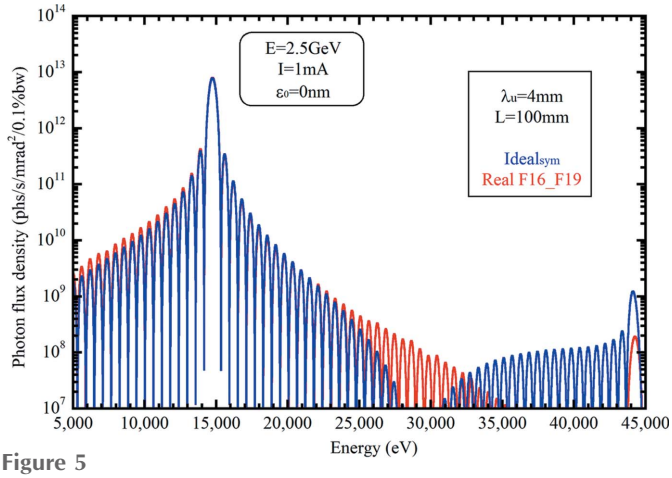

Figure 5
The spectrum calculated on the basis of the measured field for the 100 mm-long PMMs (Fig. 3) is compared with that of the ideal field for a 2.5 GeV electron beam with zero emittance and zero energy spread.

between the measurement and the calculation with the two effective poles, and believe that it is due to incomplete magnetization of the adjacent N- and S-poles in the real PMM. This problem should be resolved by improvement of the magnetizing method including reform of the structure of the present magnetizing head.

To examine the present magnetic field, the flux-density spectrum was calculated on the basis of the measured data. A calculation was made for the conditions of 2.5 GeV electron energy, zero emittance and zero energy spread. Fig. 5 shows a comparison between the spectrum at a gap of 1.6 mm and that with the ideal field of the same strength. It is noted that the radiation emitted from the present undulator field (red curve) compares well with that emitted from an ideal magnetic field (blue curve) in the region of the fundamental radiation. Nevertheless, the discrepancy is large in the third-harmonic region. However, the flux density of the third harmonic is four orders of magnitude lower than that of the fundamental. It is not practical to think about using the higher harmonic radiation from the present a-few-millimetre-period magnetic field based on the PMM. For the conditions in Fig. 5, the fundamental radiation from 10 to 15 keV should be useful for synchrotron radiation experiments.

4. Construction of the undulator frames for practical use

In order to install the PMMs with a-few-millimetre-period lengths, we designed and constructed an undulator mechanical frame (Yamamoto, 2018), shown in Fig. 6. This frame allows installing PMMs with a total length up to 200 mm. It has a vacuum chamber for the in-vacuum undulator.

Due to the small size of the undulator magnets achieved in the present study, the size of the mechanical frame of the undulator could be reduced substantially in comparison with ordinary undulators. The magnetic attractive force between the magnet-mounting girders (MGs) is also reduced, largely due to the small size of the undulator magnets. The magnetic

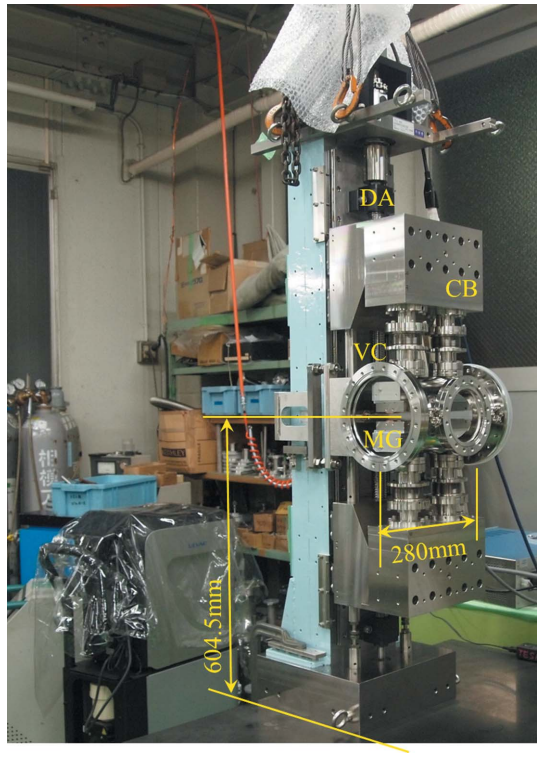

Figure 6
Photograph of the mechanical frame of the undulator with a-few-millimetre-period lengths which is able to accommodate PMMs with a total length up to 200 mm. Linear motion of the cross beam (CB) driven by the drive axis (DA) of the mechanical frame is transmitted through bellows couplings to magnet-mounting girders (MG) in the vacuum chamber (VC).

force is estimated to be as small as 36 N at a gap of 1.6 mm (86 N at a gap of 1.0 mm). The reduced magnetic force facilitates, further, to make the mechanical frame light-weight, small and slender while maintaining mechanical accuracy. The gap accuracy of the frame is as good as 0.1×10^{-6} m.

Linear motion of the cross beam driven by the drive axis of the mechanical frame is transmitted through bellows couplings to magnet-mounting girders in the vacuum chamber. The installation of the PMMs is illustrated in Fig. 7. A 100 mm-long PMM is mounted on the magnet holder with Cu masks used to protect the magnets against electron beam bombardment. The magnet holders are then placed on the magnet-mounting girder. The direction of the electron beam is shown by a green arrow in Fig. 7.

5. First observation of synchrotron radiation from the 4 mm-period undulator

5.1. Electron beam source

Generation of synchrotron radiation from the 4 mm-period undulator was demonstrated with the test Accelerator as a Coherent Terahertz Source (t-ACTS) at the Research Center for Electron Photon Science (ELPH), Tohoku University, Japan (Kashiwagi *et al.*, 2014, 2016, 2018; Hama *et al.*, 2011, 2017). The accelerator system consists of a specially designed

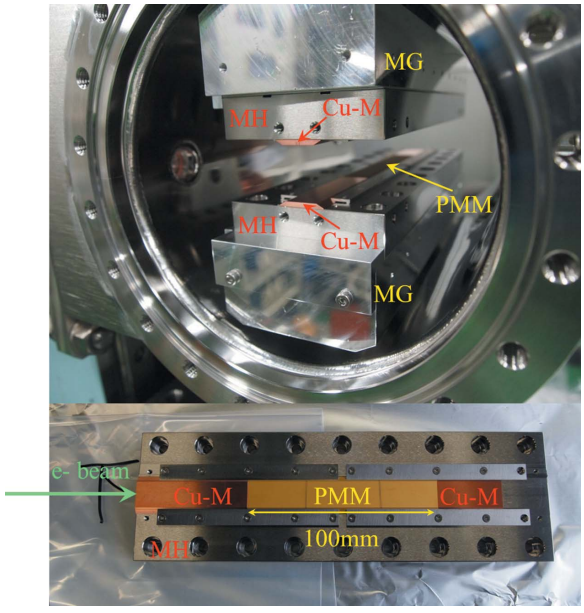

Figure 7
Installation of the PMM. A 100 mm-long PMM is mounted on the magnet holder (MH) with Cu masks (Cu-M).

S-band radiofrequency gun (Hinode *et al.*, 2010), an alpha-magnet with an energy slit, a 3 m-long S-band accelerating structure, and a beam transport line. The t-ACTS injector system can deliver electron beams with small emittance and short bunches by implementing the velocity bunching scheme, where a traveling accelerating structure is used as a bunch compressor (Serafini & Ferrario, 2001). In the present beam experiment, an electron beam was accelerated on crest-phase without any pulse compression. A macro-pulse of the electron beam contained about 5700 micro-pulses with 350 ps time interval (t_b) and the macro-pulse length was 2.0×10^{-6} s. The charge of each micro-pulse (Q_b) was typically 3.5 pC and the instantaneous beam current (Q_b/t_b) was about 10 mA. In this experiment, the beam repetition rate was set to 2 Hz.

Fig. 8 shows the beamline layout of the t-ACTS accelerator system. The 4 mm-period undulator was installed in the beam transport line. A beam diagnostic section was placed downstream of the accelerating structure. The beam emittance and Twiss parameters were measured by the quadrupole scan method using the beam profile monitor with an aluminium-coated mirror, which enabled beam size measurements of the

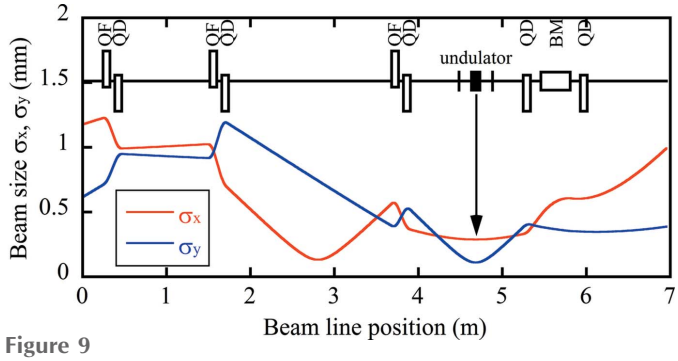

Figure 9
Electron beam size along the t-ACTS transport from accelerator exit to beam dump.

electron beam with the optical transition radiation. The Twiss parameters were adjusted so that a beam waist minimum was formed at the longitudinal center of the 4 mm-period undulator. In this experiment, the Twiss parameters were set to be $\alpha_x = \alpha_y = 0$, $\beta_x = 1.0$ m and $\beta_y = 0.17$ m at the center of the undulator. The normalized emittances in the horizontal and vertical directions were, respectively, measured to be 5.0×10^{-6} m and 4.4×10^{-6} m. The expected beam sizes were approximately 0.29 mm and 0.11 mm at the longitudinal center of the undulator. Fig. 9 shows the electron beam size in the horizontal and vertical directions. The electron beam energy was measured with a beam profile monitor at the end of the beamline, and the energy and energy spread were approximately 33 MeV and 0.44% (r.m.s.), respectively.

5.2. Observation of the blue light emission from the 4 mm-period undulator

The synchrotron radiation from the 4 mm-period undulator was observed by using the optical system shown in Fig. 10. The undulator radiation beam was switched alternatingly by a horizontal mirror through an iris in two directions and analyzed by two detectors: a color CCD camera set on-axis, and an imaging spectrometer. The iris, with a diameter of 9 mm, was placed after the extraction window. The horizontal mirror was positioned in the beam axis to direct the undulator radiation towards the spectrometer. The profile of the undulator radiation was observed by the color CCD camera (Basler, acA1300-30gc), the lens system of which was focused on the surface of an extraction window for the radiation and

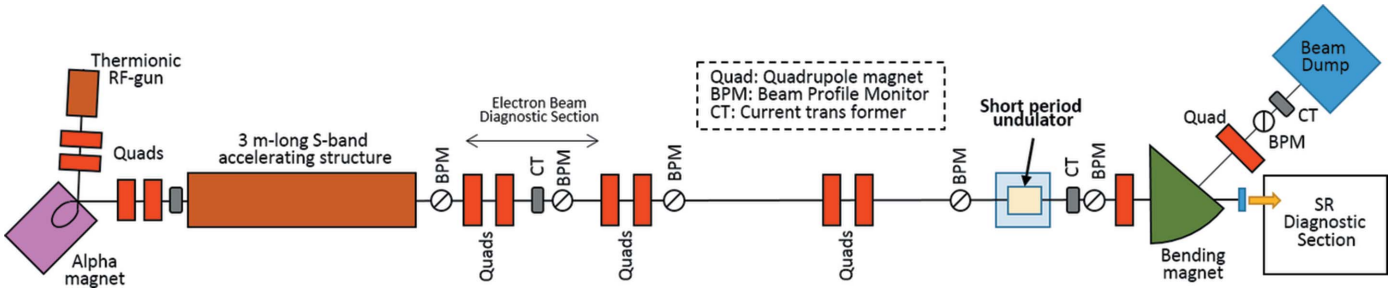

Figure 8
Layout of the t-ACTS beamline.

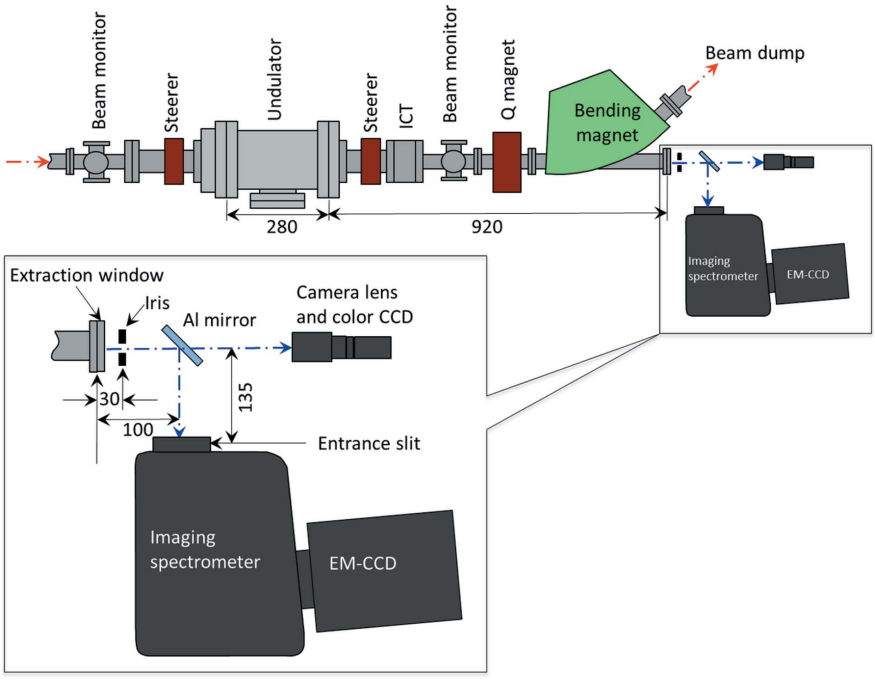

Figure 10
Layout of the optical system for observing the undulator radiation. The undulator radiation was extracted through a window and an iris. A color CCD with a camera lens was placed downstream of the iris to observe the radiation profile. A movable aluminium mirror was positioned after the iris to switch the undulator radiation into an imaging spectrometer. The geometrical arrangement is given in the figure. An EM-CCD camera that is mounted on the exit of the spectrometer is used to obtain the spectroscopic image.

synchronized to the timing of the t-ACTS accelerator which operated at a 2 Hz cycle. Fig. 11(*a*) shows the profile of the radiation which was emitted from the 'monolithic' undulator magnets with 4 mm-period length at a gap of 1.5 mm. The peripheral parts of the profile were masked with the iris, and the on-axis blue light was observed.

Spectroscopic measurements were made by using the imaging spectrometer (IsoPlane-160; Princeton Instruments) equipped with the EM-CCD camera with an electron multiplying (EM) function for high-sensitivity measurements (ProEM-HS: 1024BX3; Princeton Instruments). The signal of the detected undulator radiation was stored by the EM-CCD camera. The active area of the CCD was 1024 (horizontal) × 1024 (vertical) pixels: the pixel size was 0.013 mm × 0.013 mm. Spectroscopic data were shown as the number of photons acquired on each pixel, with the horizontal position of the CCD plane corresponding to the wavelength of the undulator radiation, and the vertical position corresponding to the vertical divergence angle from the light axis. In the horizontal axis the pixel position could be converted to wavelength with calibration based on a standard Hg lamp. Absolute sensitivity to the photon flux was obtained by using a standard halogen lamp and a He–Ne laser. The relative wavelength dependence was calibrated by the halogen lamp and an absolute calibration was made at a wavelength of 543.5 nm by the He–Ne laser.

The undulator radiation extracted by the horizontal mirror was introduced into the spectrometer through its entrance slit limiting horizontal acceptance. The undulator radiation was then analyzed at every shot of the radiation by synchronizing the acquisition time to the macro pulse of the electron beam from the t-ACTS accelerator. The exposure time of the EM-

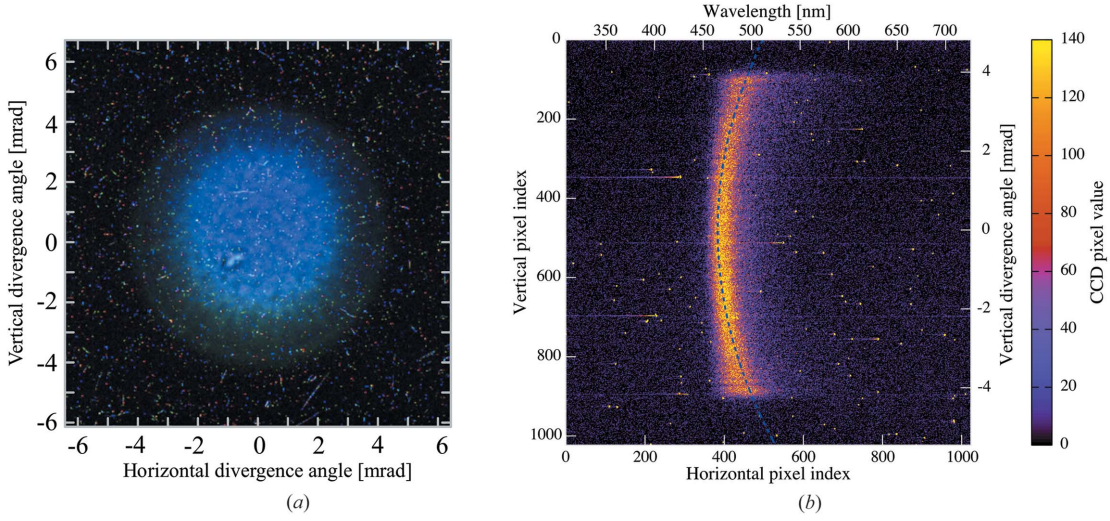

Figure 11
(*a*) The two-dimensional profile of the undulator radiation observed by the color CCD camera. (*b*) A single-shot two-dimensional spectroscopic image of undulator radiation when the undulator gap was 1.5 mm. Horizontal and vertical pixel positions correspond to the wavelength and vertical divergence angle of the radiation, respectively. The bright line forming an arc represents the undulator radiation. The dotted curve shows the angle dependence of the radiation wavelength. The top and bottom of the radiation image was cut by an iris with a diameter of 9 mm. CCD pixel values are represented by the color bar.

CCD was set to 0.001 s, sufficiently longer than the pulse length of the electron macro pulse (2.0×10^{-6} s). The gain of the EM-CCD was set to 100 throughout the spectroscopic measurements.

An example of the two-dimensional image data is shown in Fig. 11(*b*) when the undulator gap was 1.5 mm. The dotted line along the bright arc on the image represents the nature of the undulator radiation given in equation (1) (Hofmann, 1978). Hereafter we pay attention to the on-axis intensities of the undulator radiation, which are given by the spectroscopic data along the horizontal axis of the EM-CCD image. The on-axis radiation was observed at undulator gaps of 1.5, 1.7 and 2.0 mm in this experiment. After a numerical treatment for noise reduction based on the median filtering method, typical undulator spectra of the first harmonic which peak at around 2.65 eV are shown for these gaps in Fig. 12. It should be noted that the undulator based on the 100 mm-long PMM with 4 mm-period length was able to provide radiation in the visible spectral region by using a low-energy accelerator with energy less than 50 MeV such as the t-ACTS. In the present experiment, the width of the entrance slit was set to be 0.1 mm, which was small enough to neglect errors in the photon energy due to the acceptance angle of $\pm 39 \times 10^{-6}$ rad in the present measurement geometry. In Fig. 12, the horizontal axis is converted from the radiation wavelength (nm) to the photon energy (eV), and the vertical axis is also converted to the angular flux-density unit [photons s^{-1} $mrad^{-2}$ (0.1% bandwidth)$^{-1}$] which is common practice in synchrotron radiation science.

In order to avoid confusion due to shot-by-shot energy distribution in the electron beam, we selected five spectroscopic data sets at each gap with the highest energy distribution among several tens of data sets acquired. Fig. 12 shows the measured and calculated spectra. By selecting an electron energy of 33.49 MeV at a gap of 1.5 mm, 33.53 MeV at a gap of 1.7 mm, and 33.57 MeV at a gap of 2.0 mm, a characteristic of the measured spectra can be explained roughly by the calculated spectra obtained on the basis of the measured parameter set of the electron beam of the t-ACTS. The calculated spectra are denoted by the thick dotted curve at each gap. Small differences in the electron energy are due to energy fluctuation in the electron beam. As mentioned above, the absolute sensitivity of the detectors used for the photon flux measurement was calibrated by using a standard halogen lamp and a He–Ne laser. We find that the calculated spectrum agrees with the measured spectra (Fig. 12) within the limit of the shot-by-shot fluctuations in the absolute scale of the flux density.

The small number of the undulator period (= 25) used in the present study might make the defect of the undulator less critical. Our next target should be production of a longer magnetic field with a larger number of periods. We have started efforts in this direction and have attempted to obtain a long undulator field by connecting several PMMs. Key points for this development are to suppress the field error at the connection points and also to suppress the variation of the deflection parameter at each PMM, as small as possible. For

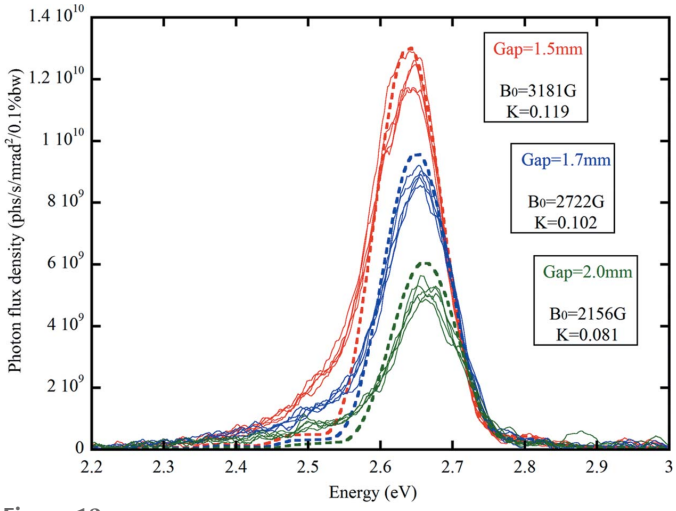

Figure 12
Measured and calculated undulator spectra (flux density) of the first harmonic of the undulator radiation from the 4 mm-period undulator with 100 mm length. Five spectroscopic data sets with the highest energy distribution among several tens of data sets acquired at gaps of 1.5, 1.7 and 2.0 mm are shown. The calculated spectra are denoted by the thick dotted curves for each gap. The calculations were made on the basis of the measured parameter set of the electron beam of the t-ACTS, by selecting an electron energy of 33.49 MeV at a gap of 1.5 mm, 33.53 MeV at a gap of 1.7 mm, and 33.57 MeV at a gap of 2.0 mm.

this purpose, we have developed a new connection method for the PMMs and succeeded in fabricating a longer undulator with the number of period up to 125 which has a 500 mm magnet length (= 5 × 100 mm-long PMM) (Yamamoto, 2018). We found that the above-mentioned suppressions are very effective in this new method.

Some discrepancies were found in the lower-energy part of the undulator spectra. Because the electron beam having a finite vertical beam size of σ_y = 0.11 mm passes through the short gap of 1.5–2.0 mm, it should feel the vertical variation of the magnetic field. We investigated the effect of the two-dimensional magnetic field variation in the electron beam on the undulator spectrum. However, we found that the effect was negligibly small since the change in the deflection parameter was too small, due to the 4 mm-period length, to affect the shape of the spectrum although there is definite spatial variation in the magnetic field. The above discrepancy in the spectra may be due to a low-energy component in the electron beam unknown in the present observation. This fact may require further efforts to understand the discrepancy not only from the accelerator side but also from the undulator side. It also indicates the possible importance of the present a-few-millimetre-period undulator not only as a light source for experimental use but also as a monitor for appropriate operation of the accelerators.

6. Conclusion

The present results indicate that we are heading in the right direction for the development of undulators with a period length of a few millimetres. We have established an effective and reliable method for fabricating PMMs with a-few-milli-

metre-period lengths. A very stable and high-quality undulator field with 4 mm-period length was produced in the gap between opposing PMMs. We have a strong perspective to fabricate a longer undulator as reported elsewhere (Yamamoto, 2018). Still we have several issues to overcome including production of a higher value of the deflection parameter and realization of a very short gap of ∼1 mm. For the former we have been continuing to improve the magnet design; another possibility is the introduction of cryogenic undulator technology (Hara *et al.*, 2004). For the latter we expect advances in accelerator science enabling a very short gap for the a-few-millimetre period undulators. We have already started a design study in order to construct a light source accelerator which is optimized for the present a-few-millimetre-period undulators (Ohkuma & Yamamoto, 2017).

A mechanical frame for in-vacuum-type undulators was designed and constructed to install the 100 mm-long PMMs. Experiments to observe the synchrotron radiation emitted from the 4 mm-period undulator based on real electron beams were conducted using the S-band linac, t-ACTS at the ELPH, Tohoku University, Japan. The first observation and characterization of blue light was accomplished successfully.

Funding information

The following funding is acknowledged: Japan Society for the Promotion of Science (grant No. KAKENHI 24651107); Japan Society for the Promotion of Science (grant No. KAKENHI 26246044); ImPACT Program of Council for Science, Technology and Innovation (Cabinet Office, Government of Japan).

References

Benabderrahmane, C., Valléau, M., Ghaith, A., Berteaud, P., Chapuis, L., Marteau, F., Briquez, F., Marcouillé, O., Marlats, J.-L., Tavakoli, K., Mary, A., Zerbib, D., Lestrade, A., Louvet, M., Brunelle, P., Medjoubi, K., Herbeaux, C., Béchu, N., Rommeluere, P., Somogyi, A., Chubar, O., Kitegi, C. & Couprie, M.-E. (2017). *Phys. Rev. Accel. Beams*, **20**, 033201.

Calvi, M., Schmidt, Th., Anghel, A., Cervellino, A., Leake, S. J., Willmott, P. R. & Tanaka, T. (2013). *J. Phys. Conf. Ser.* **425**, 032017.

Casalbuoni, S., Cecilia, A., Gerstl, S., Glamann, N., Grau, A. W., Holubek, T., Meuter, C., Saez de Jauregui, D. & Voutta, R. (2016). *Phys. Rev. Accel. Beams*, **19**, 110702.

Chavanne, J., Benabderrahmane, C., Le Bec, G. & Penel, C. (2015). *Synchrotron Radiat. News*, **28**(3), 15–18.

Chavanne, J., Penel, C., Plan, B. & Revol, F. (2003). *Proceedings of the 2003 Particle Accelerator Conference (PAC2003)*, 12–16 May 2003, Portland, OR, USA, pp. 253–255. TOPA013.

Halbach, K. (1981). *Nucl. Instrum. Methods Phys. Res.* **187**, 109–117.

Hama, H., Abe, T., Kashiwagi, S., Hinode, F., Muto, T., Nanbu, K., Takahashi, K., Nagasawa, I., Kanomata, K., Saito, H. & Saito, Y. (2017). *Int. J. Opt. Photon. Eng.* **2**, 004.

Hama, H., Kawai, M., Kashiwagi, S., Hinode, F., Miyahara, F., Nanbu, K., Muto, T., Tanaka, Y., Li, X. & Huang, N. (2011). *Energy Proc.* **9**, 391–397.

Hara, T., Tanaka, T., Kitamura, H., Bizen, T., Maréchal, X., Seike, T., Kohda, T. & Matsuura, Y. (2004). *Phys. Rev. ST Accel. Beams*, **7**, 050702.

Hara, T., Tanaka, T., Tanabe, T., Maréchal, X.-M., Okada, S. & Kitamura, H. (1998). *J. Synchrotron Rad.* **5**, 403–405.

Hendel, S., Schäfers, F., Hävecker, M., Reichardt, G., Scheer, M., Bahrdt, J. & Lips, K. (2016). *AIP Conf. Proc.* **1741**, 030038.

Hinode, F., Hama, H., Kashiwagi, S., Kawai, M., Nanbu, K., Miyahara, F., Muto, T., Oohara, H. & Tanaka, Y. (2010). *Proceedings of the First International Particle Accelerator Conference (IPAC2010)*, 23–28 May 2010, Kyoto, Japan, pp. 1731–1733. TUPEC010.

Hofmann, A. (1978). *Nucl. Instrum. Methods*, **152**, 17–21.

Ivanyushenkov, Y., Harkay, K., Abliz, M., Boon, L., Borland, M., Capatina, D., Collins, J., Decker, G., Dejus, R., Dooling, J., Doose, C., Emery, L., Fuerst, J., Gagliano, J., Hasse, Q., Jaski, M., Kasa, M., Kim, S. H., Kustom, R., Lang, J. C., Liu, J., Moog, E., Robinson, D., Sajaev, V., Schroeder, K., Sereno, N., Shiroyanagi, Y., Skiadopoulos, D., Smith, M., Sun, X., Trakhtenberg, E., Vasserman, I., Vella, A., Xiao, A., Xu, J., Zholents, A. & Gluskin, E. (2015). *Phys. Rev. ST Accel. Beams*, **18**, 040703.

Kashiwagi, S., Abe, T., Saito, H., Hinode, F., Kanomata, K., Miura, S., Muto, T., Nagasawa, I., Nanbu, K., Ninomiya, S., Nishimori, N., Saito, Y., Takahashi, K. & Hama, H. (2018). *Infrared Phys. Technol.* **93**, 335–339.

Kashiwagi, S., Hinode, F., Muto, T., Shibasaki, Y., Nanbu, K., Takahashi, K., Nagasawa, I., Nagasawa, S., Tokoku, C., Lueangaramwong, A. & Hama, H. (2014). *Proceedings of the 27th Linear Accelerator Conference (LINAC2014)*, 31 August–5 September 2014, Geneva, Switzerland, pp. 1178–1181. THPP136.

Kashiwagi, S., Nagasawa, F., Hinode, T., Muto, H., Saito, T., Abe, K., Nanbu, I., Nagasawa, K., Takahashi, C., Tokoku, E., Kobayashi, E. & Hama, H. (2016). *Energy Proc.* **89**, 346–352.

Ohkuma, H. & Yamamoto, S. (2017). *Proceedings of the 14th Annual Meeting of the Japanese Particle Accelerator Science (PASJ2017)*, 1–3 Aug 2017, Sapporo, Japan, pp. 221–225. THOL12. (In Japanese.)

Otake, Y. (2012). *Proceedings of the 26th International Linear Accelerator Conference (LINAC2012)*, 9–12 September 2012, Tel Aviv, Israel, pp. 427–431. TU2A02.

Serafini, L. & Ferrario, M. (2001). *AIP Conf. Proc.* **581**, 87–106.

Tanabe, T., Bassan, H., Broadbent, A., Cappadoro, P., Escallier, J., Harder, D., Hetzel, C., Hidas, D., Kitegi, C., Kosciuk, B., Musardo, M. & Kirkland, J. (2017). *J. Synchrotron Rad.* **24**, 919–924.

Tanaka, T., Goto, S., Hara, T., Hatsui, T., Ohashi, H., Togawa, K., Yabashi, M. & Tanaka, H. (2012). *Phys. Rev. ST Accel. Beams*, **15**, 110701.

Wallén, E., Blomqvist, I., Johansson, U. & Jensen, B. N. (2006). *Proceedings of the Tenth European Particle Accelerator Conference (EPAC2006)*, 26–30 June 2006, Edinburgh, Scotland, pp. 3607–3609. THPLS137.

Yamamoto, S. (2013). *J. Phys. Conf. Ser.* **425**, 032014.

Yamamoto, S. (2014). *Proceedings of the 5th International Particle Accelerator Conference (IPAC2014)*, 15–20 June 2014, Dresden, Germany, pp. 1845–1847. WEOAA02.

Yamamoto, S. (2015). *Synchrotron Radiat. News*, **28**(3), 19–22.

Yamamoto, S. (2016). *AIP Conf. Proc.* **1741**, 020029.

Yamamoto, S. (2018). *Proceedings of the 9th International Particle Accelerator Conference (IPAC2018)*, 29 April–4 May 2018, Vancouver, BC, Canada, pp. 1735–1739. WEXGBD1.

Yamamoto, S., Shioya, T., Hara, M., Kitamura, H., Zhang, X. W., Mochizuki, T., Sugiyama, H. & Ando, M. (1992). *Rev. Sci. Instrum.* **63**, 400–403.

Yamamoto, S., Tsuchiya, K., Sasaki, H., Aoto, T., Shioya, T., Garrett, R., Gentle, I., Nugent, K. & Wilkins, S. (2010). *AIP Conf. Proc.* **1234**, 599–602.

Yamamoto, S., Tsuchiya, K. & Shioya, T. (2007). *AIP Conf. Proc.* **879**, 384–387.

Yamamoto, S., Zhang, X. W., Kitamura, H., Shioya, T., Mochizuki, T., Sugiyama, H., Ando, M., Yoda, Y., Kikuta, S. & Takei, H. (1993). *J. Appl. Phys.* **74**, 500–503.